# BEAM DISPLACEMENT AND REFLECTION IMAGES IN THE BELLHOP GAUSSIAN BEAM MODEL

Dale D. Ellis[a], Diana F. McCammon[b]

[a] Dale Ellis Scientific Inc., Dartmouth, NS, Canada
[b] 475 Baseline Road, Black Rock, NS, B0P 1V0 Canada

Contact: Dale D. Ellis, 18 Hugh Allen Drive, Dartmouth, NS, B2W 2K8 Canada;
email: daledellis@gmail.com

***Abstract:*** *The objective of this paper is to describe the behavior of the Bellhop Gaussian Beam Model when beam displacement terms and boundary reflection images are included. Beam displacement is a horizontal shift of the reflected ray at sub-critical angles from a hard bottom caused by the reflection's phase delay. Beam displacement primarily affects the phase of the field. Boundary reflection images augment the central ray with surface and bottom image beams and primarily affect the level of the field. The goal is to determine if these terms will improve the low-frequency, shallow water performance of the Gaussian beam model. Our approach is to measure the validity of Bellhop's Gaussian Beam Model predictions at water depth/wavelength (h/λ) ratios smaller than the usually ascribed Bellhop limitation of h/λ > 20 by comparing the resulting intensity predictions with a normal mode exact solution PROLOS. The conclusion of this examination shows that the inclusion of beam displacement and boundary image beams does greatly enhance the low-frequency shallow water accuracy of Bellhop.*

***Keywords:*** *beam displacement, reflection images, ray/mode comparisons*

## 1. INTRODUCTION

It is commonly accepted that ray theory is accurate in a high-frequency regime where the water depth/wavelength ratio $h/\lambda \gg 1$. In practice, the ray model Bellhop suggests its validity extends down to $h/\lambda > 20$. As there is a need for a valid model in shallow water at low frequencies that is fast and includes range dependence, it would be advantageous to extend the range of Bellhop to lower frequencies where the boundaries, particularly the bottom interface, are intrusive. One extension to ray theory is to include the phase of the bottom's reflection coefficient in the stationary phase evaluation of the Helmholtz integral. This extension is called "beam displacement". Beam displacement refers to the lateral displacement of the ray path when it intersects the bottom at sub-critical angles. It is expressed mathematically as the change of the reflection phase with respect to wavenumber and the equation for the horizontal displacement of the ray is a complicated function of frequency, grazing angle, sediment sound speed and density. A second extension to ray theory in the immediate proximity to the boundaries is to allow the Gaussian beam's spatial extent to ensonify the receiver both before and after reflection using 'image beams' that contribute coherently to the central ray. Statistical comparisons of the correlation and mean error between these extensions and an exact solution will be presented that show improvements in accuracy.

## 2. MATHEMATICS

### 2.1 Gaussian Beams

Gaussian Beams are constructed using the standard ray tracing systems of equations for describing the path of the central ray in the beam and therefore its phase. A second system of equations is defined for determining the extent of spread of the beam about the central ray that provides the magnitude of the pressure. This latter set of equations defines a beamwidth parameter q which appears in the pressure in the Gaussian Weighting function and an amplitude term, $\exp[n^2/2Bq^2] / \sqrt{q}$, where B is a constant related to the ray angle spacing and n is the normal distance from the ray to the receiver depth. A simple expression for q is found in closed form for a linear SSP as:

$$q = (\sin\theta_a - \sin\theta)/(gD^2) \quad (1)$$

where $\theta_a$ is the angle at the start of a ray step within a SSP layer and $\theta$ is the angle at the end of the step within that same layer. The symbol g is the constant gradient of the layer and D is Snell's constant $D = \cos\theta_0/c_0$. It can be seen that a caustic will be formed whenever the ray is nearly horizontal in the layer, so that $q \sim 0$. Additional terms must be added to q to satisfy continuity conditions whenever the beam traverses into a new SSP layer or reflects from a boundary. Details of these terms can be found in [1] where they are called 'jump conditions', but these details are not important to the study in this paper, so are not included here.

Because there can be large changes in q from step to step, the variable is interpolated according to the distance the ray has travelled between steps based on the location of the ray normal n between the ray and the receiver point (see Fig. 1). The interpolating fraction

is the proportional distance along the ray from the $i$-1$^{th}$ step to the normal and is used to interpolate the values of the intensity factor q and the ray time delay τ which determines the ray phase.

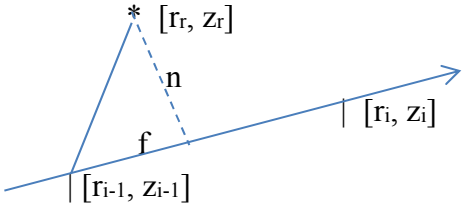


*Fig. 1: Drawing of the relative positions of the ray steps in range and depth with relation to the receiver position [$r_r$, $z_r$], the interpolation fraction* f *and the normal distance* n.

## 2.2 Beam Displacement

According to [2], the reflection coefficient and phase from the sediment below the critical angle are:

$$\Re = \frac{(\rho_2\gamma_1 - i\,\rho_1\gamma_2)}{(\rho_2\gamma_1 + i\,\rho_1\gamma_2)}, \qquad \phi = -2\tan^{-1}(\rho_1\gamma_2/\rho_2\gamma_1), \tag{2}$$

where the densities are $\rho$ and the vertical wavenumbers are $\gamma$. The technique of stationary phase provides the range, Δ, traveled by this ray while being reflected, hence the term beam displacement. The equation for Δ is obtained from the derivative of the phase with respect to the wavenumber $k$. It may be written as:

$$\Delta = \frac{2\,\rho\, ctn\theta\,(1-\zeta^2)}{k\sqrt{b}\,d}, \tag{3}$$

where the symbols are defined as $\rho = \rho_2/\rho_1$, $\zeta = c_1/(c_2 - i\alpha)$, $b = cos\theta^2 - \zeta^2$, and $d = \rho^2\, sin^2\theta + b$. Beam displacement is included in Bellhop [3]. In this form, it is easy to identify the dependence on frequency, grazing angle and critical angle. The displacement will increase as frequency is lowered because of the wavenumber factor in the denominator. The displacement will also increase as the grazing angle becomes shallower because of the cotangent dependence in the numerator. Finally, the displacement will increase as the grazing angle approaches the critical angle when the term $b$ under the square root in the denominator will approach zero. Thus, there is a minimum formed between zero grazing and the critical angle.

One insightful method for understanding beam displacement is the effective depth approximation [4], illustrated below in Fig. 2 where a depth $\Delta H$ is defined into the sediment to allow the ray to 'turn'.

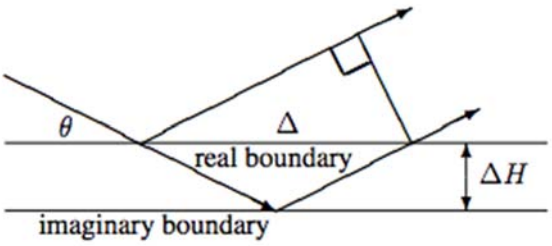


*Fig. 2: Diagram of effective depth ΔH, and beam displacement* Δ.

Using this physical approach, the beam displacement from the effective depth approximation produces an equation very similar to Eq. 3. It has the correct low-angle behavior and is infinity at zero grazing angle, but it doesn't have the correct behavior near the critical angle because it lacks the term $\sqrt{\boldsymbol{b}}$ in the denominator, as shown in Fig. 3. Thus, the phases of rays near the critical angle will be slightly off under this approximation.

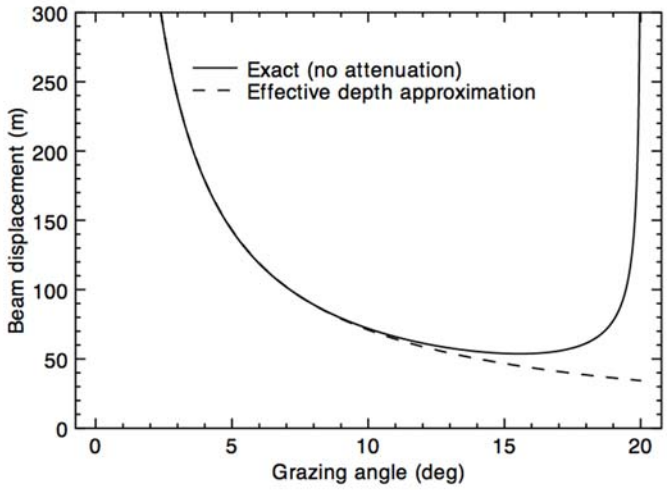


*Fig. 3: Beam displacement: exact (solid line), effective depth approximation (dashed line).*

The inclusion of sloping bathymetry is discussed in [5]. A ray plot of two rays, the 2° and the 0.5° rays, is shown in Fig. 4 where the sound speed profile is downward refracting and the bathymetry is given a uniform slope from 50 m to 80 m over 10 km (a 0.17° slope angle). The beam displacement is large at these shallow angles and one can see the increase in displacement as the depth of the bottom increases which makes the grazing angle shallower.

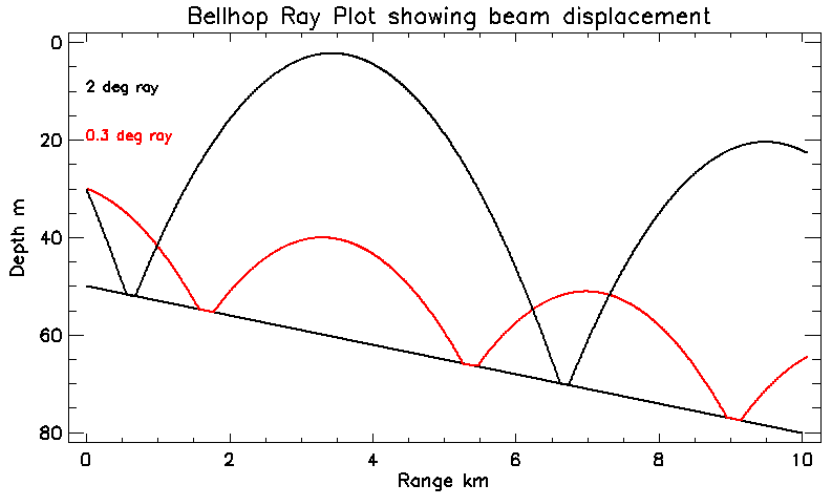


*Fig. 4: Ray trace showing the beam displacement for two shallow rays in a downward refracting profile over a downward sloping bottom. The displacement is significant for very shallow grazing rays.*

In ray theory, the additional time delay associated with the ray's travel through the sediment is computed as:

$$\tau_{\Delta} = \Delta \frac{cos\theta}{c}. \tag{4}$$

This extra delay proves critically important to obtaining phase matching with normal mode theory.

### 2.3 Image Beams

Image beams are defined as the mirror image of the ray above and below the boundaries. This means the ray location is changed but all the quantities obtained from the ray tracing (in particular, q and τ) remain the same. For the surface-reflected image, the ray within the water column at step *i-1* has the position $[r_{i-1}, z_{i-1}]$, and the image ray above the surface has the step position $[r_{i-1}, -z_{i-1}]$ as shown in Fig 5. An extra reflection coefficient and phase are added to the amplitude and phase of the pressure of the image ray. In the case of the surface reflection, the reflection phase is π. This is equivalent to subtracting the image from the eigenray, which in turn makes the pressure zero when the receiver is exactly at the surface, as required by the boundary conditions for a pressure release surface. The remaining assembly of the ray intensity contribution proceeds just as it had with the water column ray, using the interpolating fraction $f_s$ to compute the contributions of beamwidth q and time delay τ from the stepped interval of the ray.

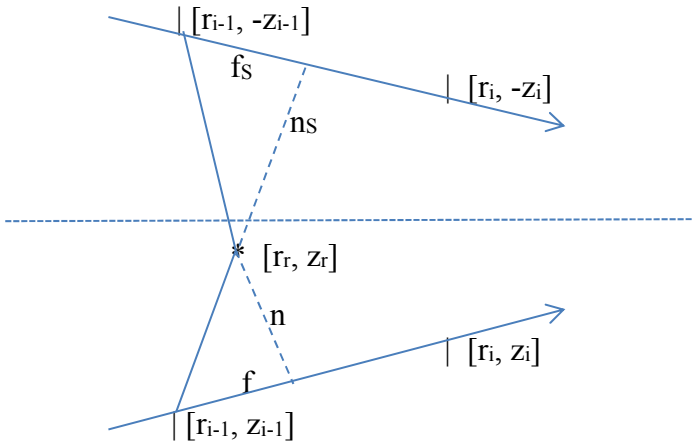


*Fig. 5: Ray and image ray above the surface. Ray steps differ by the sign of the ray depth. Interpolating fraction* $f_s$ *and normal* $n_s$ *will equal* f *and* n *whenever the receiver point is on the boundary.*

For the bottom image (invert Fig. 5), the procedure is the same except the *i-1* step of the ray position of the image below the bottom of depth *H* has the position $[r_{i-1}, 2H - z_{i-1}]$. In this case, the interpolating fraction must be adjusted to remove the factor of 2H. For the bottom image ray, another reflection coefficient and phase from the sediment are added to the amplitude and phase of the pressure, computed using the ray angle at the *i-1*$^{th}$ step.

## 3. COMPARISON OF TL WITH BEAM DISPLACEMENT AND IMAGES

The Pekeris environment chosen for these tests is that given in [2]. It consists of an isospeed water column with speed $c_1$ = 1508 m/s; a water depth of 50 m; sand bottom with density $\rho_2$ = 1.25, sound speed $c_2$ = 1605 m/s, and attenuation $\alpha_2$ = 0.11 dB/mkHz; with the critical angle $\theta_{crit} = cos^{-1}(c_1/c_2) = 20.0216°$**.** The normal mode results were trivial to reproduce using PROLOS, a normal mode code [6]. At frequency f = 140 Hz there are 3

trapped modes with phase speeds and grazing angles: $v_1$ = 1514.9595 m/s; $\theta_1$ = 5.4940°; $v_2$ = 1536.4097 m/s; $\theta_2$ = 11.0354°; $v_3$ = 1573.6938 m/s; $\theta_3$ = 16.6135°.

### 3.1 Beam displacement

An example comparison of the exact normal mode result from PROLOS vs Bellhop's Gaussian beam prediction with and without beam displacement is shown in Fig. 6. The beam displacement causes a shift in phase of the transmission loss and the correlation between PROLOS and Bellhop increases from 0.653 to 0.826 when beam displacement is included. However, the rms DB error is about the same for both.

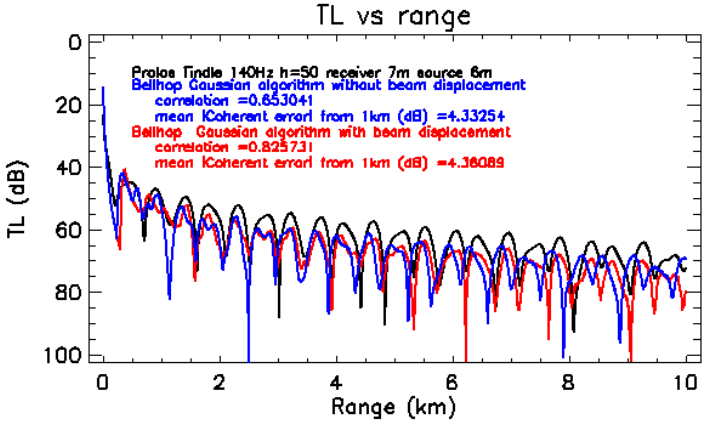


*Fig. 6: Tindle test case at 140 Hz. Black = exact (PROLOS), red = Bellhop with beam displacement, blue = Bellhop without beam displacement. Nether Bellhop run included boundary images.*

### 3.2 Boundary images

An example comparison of the exact normal mode result from PROLOS vs Bellhop's Gaussian beam prediction with and without boundary images is shown in Fig. 7. The boundary images add energy to the field and bring the exact solution and Bellhop solution in much closer level agreement. While the correlation remains essentially the same, the rms DB error falls from 4.36 dB to 1.22 dB when the boundary images are included.

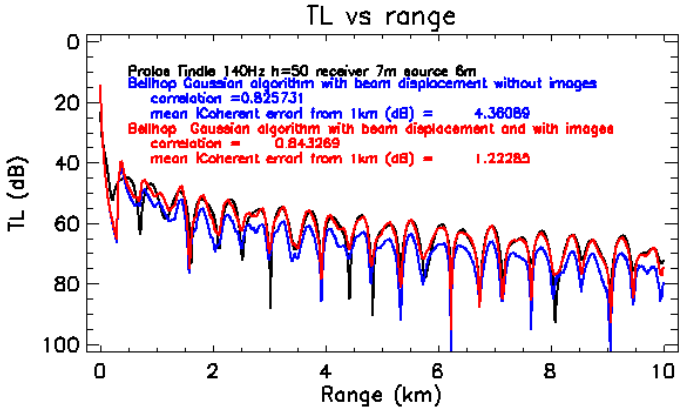


*Fig. 7: 140 Hz calculation. Black = exact (PROLOS), red = Bellhop with boundary images, blue = Bellhop without images. Both Bellhop runs included beam displacement.*

### 3.3 H/λ study with beam displacement and images

Throughout this study, it was evident that for coherent TL comparisons, both the position and the level of the structure of the TL need to be compared. Two separate statistical measures were computed to try to capture this amplitude and phase matching. Correlation measures the goodness-of-fit of peaks and nulls while mean coherent error measures level differences. In the computation of the mean error, it is important to try not to include the nulls because deep nulls (in dB) will probably not be well matched and can skew the statistic. Therefore, the data were detrended and dB level-windowed and range-windowed to exclude the short range < 1 km before the mean difference in dB was sought. This means that this statistic is not a rigorous measure of level difference and can only serve as a representation of level differences between various tests.

Fig. 8 compares the correlation coefficient between the algorithms outputs and the exact solution. Beam displacement is included in all solid curves and is absent in all dashed curves. The code with the images is shown in red, the original non-imaged code is shown in blue. It is clear that beam displacement produces a better phase match because the correlation is consistently very high. It is worth noting that data points (not plotted here) for h/λ = 13.3 (400 Hz) and 19.9 (600 Hz) were both 0.98. In addition, the code with the images is equal to or better correlated than the original as the frequency falls. Correlation remains very high, (0.94) down to h/λ = 5 after which it begins to decrease.

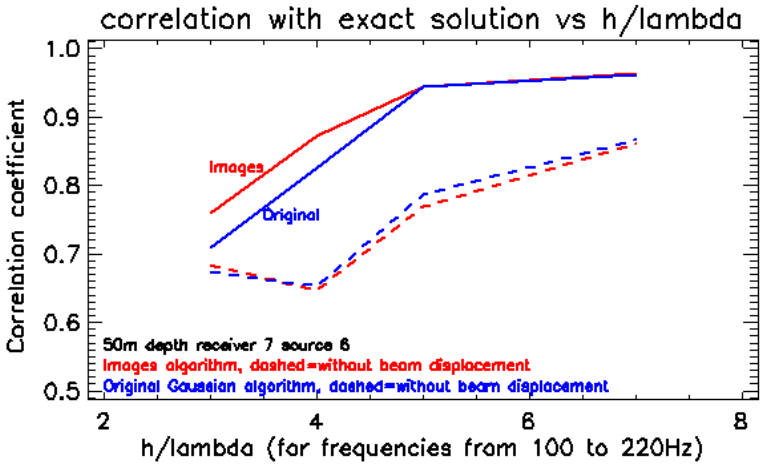


*Fig. 8: Comparison of correlation coefficients.*

Fig. 9 displays the comparisons of the mean absolute coherent error beyond 1 km. To obtain these errors, the TL was detrended in range, then windowed to exclude the deeper nulls. The errors are computed as dB differences and are intended only to provide a comparison between methods. The figure shows that the algorithm with images is consistently better, having less error than the original code. In addition, the figure shows that including beam displacement lowers the coherent errors. It appears that the most noticeable departure in all these figures occurs below 140 Hz, where h/λ = 4.6.

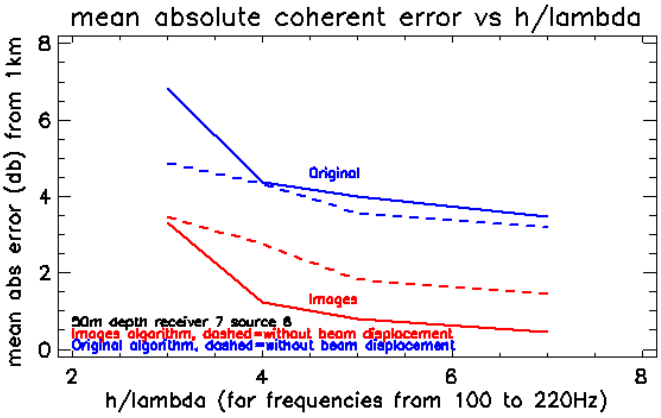


*Fig. 9: Comparison of mean absolute coherent error from 1 km as a function of h/λ.*

It appears that beam displacement provides the proper phase delay to cause the Gaussian Beam algorithm to correlate well with the exact solution in the placement of peaks and nulls, whereas the image beams provide the missing energy to raise the level to be commensurate with the exact solution. Either addition alone is not sufficient to make a good match to the exact solution, but taken together the result is a significant improvement to lower frequencies than conventional ray theory.

## 4. ACKNOWLDEGEMENTS

This work was supported by Defence Research & Development Canada, Atlantic Research Centre, Dartmouth, Nova Scotia, Canada, under the guidance and thoughtful advice of Dr. Sean Pecknold. This effort was administrated by Martin Taillefer, Maritime Way Scientific Ltd., Ottawa, Ontario. Dr. Ron Kessel provided useful comments.

## REFERENCES

[1] **M. B. Porter & H. Bucker**, Gaussian beam tracing for computing ocean acoustic fields, *J. Acoust. Soc. Am., 82(4)*, 1349–1359, 1987.
[2] **C. T. Tindle**, Ray calculations with beam displacement, *J. Acoust. Soc. Am., 73(5)*, 1581–1586, 1983.
[3] **M. B. Porter**, *The Bellhop manual and user's guide, preliminary draft.* Retrieved from Ocean acoustics library: oalib.hlsresearch.com, January 2011.
[4] **D. M. F. Chapman, P. D. Ward, & D. D. Ellis,** The effective depth of a Pekeris ocean waveguide, including shear wave effects, *J. Acoust. Soc. Am., 85*, 648–653, 1989.
[5] **C. T. Tindle & G. B. Deane,** Sound propagation over a sloping bottom using rays with beam displacement, *J. Acoust. Soc. Am., 78(4)*, 1366–1374, 1985.
[6] **D. D. Ellis,** A two-ended shooting technique for calculating normal modes in underwater sound propagation, DREA Report 85/105, Defence Research Establishment Atlantic, Dartmouth, NS, Canada, 1985.